Chalcogenide Letters Vol. 22, No. 1, January 2025, p. 1 - 9

Raman and x-ray diffraction data analysis of $Ge_2Sb_2Te_5$ films using gaussian approximation considering the temperature population factor

S. N. Garibova [a,b,*], A. I. Isayev [a], S. A. Rzayeva [a], F. N. Mammadov [c]
[a] *Institute of Physics, Ministry of Science and Education Republic of Azerbaijan, Baku, 1143, Azerbaijan*
[b] *Department of Physics and Electronics, Khazar University, Baku, 1096, Azerbaijan*
[c] *SOCAR Midstream Operations LLC, Baku, Azerbaijan*

The structure particulars of amorphous $Ge_2Sb_2Te_5$ thermally evaporated on glass substrates, as well as films annealed at temperatures of 500 and 700 K have been studied by the considering of experimentally established facts obtained from X-ray analysis and Raman spectroscopy measurements. The Debye-Scherrer and Williams-Hall methods were applied to the X-ray diffraction data for estimate the size of crystallites, interatomic distances, dislocation density and structure distortion degree. The features of heat treatment effect on numerical values of the above quantities at a given temperatures have been established. The analysis of the spectral distribution of Raman scattering was measured at light frequencies between 40 ÷ 300 cm^{-1}. The rather extended nature of the identified bands suggests the presence of several vibrational modes, leading to the appearance of individual spectral bands. To determine the vibrational modes, a reduced intensity was constructed from the experimental Raman spectrum data and the Gaussian approximation was applied to the latter. Having a mind the results of published works, the vibration modes existing in the samples obtained immediately after the process of layer application were determined, as well as the chemical nature and structure elements corresponding to these modes forming the amorphous matrix. The vibration modes in crystallized layers after heat treatment at the given temperatures were determined, as well as the chemical bonds and structural units forming their local structure.

(Received October 16, 2024; Accepted January 2, 2025)

Keywords: Chalcogenide semiconductor, Amorphous, Crystalline state, Raman spectroscopy, Gaussian fitting

1. Introduction

Binary along with multicomponent amorphous and crystalline tellurides are increasingly attracting an interest of scientists studying the fundamental properties of chalcogenide semiconductors and establishing their capability for specific area application in the electronics industry [1-10]. It is known that attractive feature of these materials is their possession of significantly differences in particulars between amorphous and ordered states. This allowed them due to phase-change effect to be used in electronic accessories as working elements that perform signal recording and erasing within nanosecond time intervals.

Short recording and erasing times, as well as high physical properties disagree between random and ordered states allowed using $Ge_2Sb_2Te_5$ (GST225) as active material for manufacture of digital storage devices [11-13]. These operations are performed through a reversible processes involving the “amorphous-crystal-liquid” phase transition of active substance under laser beam or electric pulse action. The named processes, in particular, the crystallization are followed in the structure modification along with parameter of short-range order in atoms arrangement, which is confirmed by results of work [1, 14]. Thus, unlike most non-crystalline materials, short-range structural order of amorphous and crystalline $Ge_2Sb_2Te_5$ is not the same, which determines

---

[*] Corresponding author: sqaribova1@gmail.com

https://doi.org/10.15251/CL.2025.221.1

relevance of studying the changes occurring in them during the “amorphous-crystal” phase transition state. Additionally, the striped appearance of crystallized $Ge_2Sb_2Te_5$ Raman spectrum [14-17] suggests defects in their structure which must be considered when analyzing the experimental results related to the study of the structural characteristics.

This research studies the temperature-induced variation of local structure feature in $Ge_2Sb_2Te_5$ using X-ray and Raman scattering measurements. Raman strip of both disordered and heat-treated films indicates a complex composition of the observed bands, i.e. each of them consists of several vibrational modes. To identify an individual vibrational mode, experimental data were fitted by the Gaussian method. In [15], it is shown that $Ge_2Sb_2Te_5$ films thermally deposited on unheated glass surface are amorphous, while annealed around 500 and 700 K successively become cubic and hexagonal shape. This paper interprets experimental results from X-ray diffraction and Raman scattering, considering that amorphous and crystalline GST materials differ not just in their macroscopic properties, but also in their native arrangement at short-range order. Structural evaluation of investigated $Ge_2Sb_2Te_5$ films has been processed by the uses of Debye-Scherrer [18-20] and Williams-Hall [21] methods in experimental XRD data. Local structural analysis was performed through Gaussian approximation applied to Raman spectroscopy data obtained from experiments.

2. Research methods and sample preparation

Compound based on Ge, Sb, and Te with special purity (99.999%) was synthesized in quartz ampoules that were pumped down to a pressure of 10^{-4} Torr. The process took place at 1200 K temperature for 10 hours, with a 5- hour holding period in rotating furnace, ending up turned-off to allow the cool alloy. Films of 0.5-1.5 μm thick were prepared by thermal evaporation on a cold glass substrate at 0.05 μm/min rates in 10^{-4} Torr pressure vacuum. Annealing process of the obtained films was performed in evacuated ampoules at temperatures of 500 and 700 K for 20-30 minutes. X-ray spectra of the studied films were recorded using D2Phaser diffractometer (Bruker) and CuKα source with λ=0.15406 nm radiation wavelength in 2θ=5-80° angular range. Nanofinder30 Raman microscope of λ=532 nm laser emission wavelength was used to take Raman spectra, in which CCD camera served (-70°C) as cooling system for the photodetector. The stimulus duration of 9 mW laser beam lasted 10-40 seconds.

3. Analysis of Raman spectra data of $Ge_2Sb_2Te_5$

In this work, the Raman spectra were corrected for the temperature population factor. For this purpose, the reduced (true) intensity of the lines in $Ge_2Sb_2Te_5$ film Raman spectra is found using the formula [1-2, 17]:

$$I^{red}(\omega) = (\omega_0 - \omega)^{-4}\omega[n(\omega,T) + 1]^{-1}I^{exp}(\omega)\ , \tag{1}$$

where $n(\omega,T) = (e^{\hbar\omega/kT} - 1)^{-1}$- temperature occupancy factor.

The scattered Raman shift, the spectrum corrected for the temperature factor of sample population and Gaussian approximation, respectively are shown in Figures 1-3.

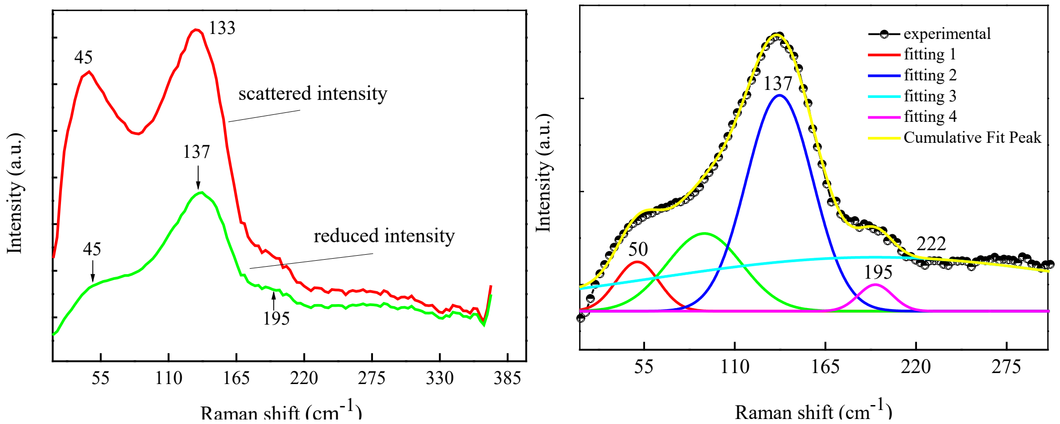

(a) *(b)*

Fig. 1. Raman spectra for $Ge_2Sb_2Te_5$ amorphous film before annealing at 300 K (a) and Gaussian fitting (b).

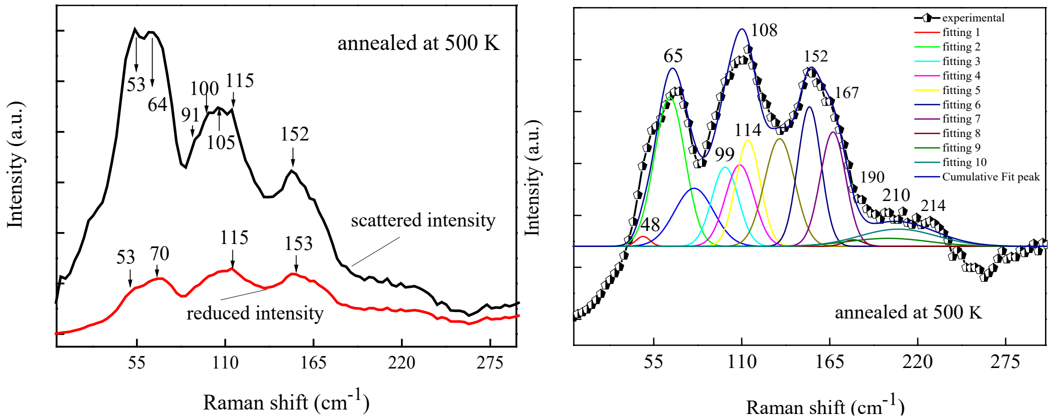

(a) *(b)*

Fig. 2. Raman spectra for $Ge_2Sb_2Te_5$ film annealed at temperature 500K (a) and Gaussian fitting (b).

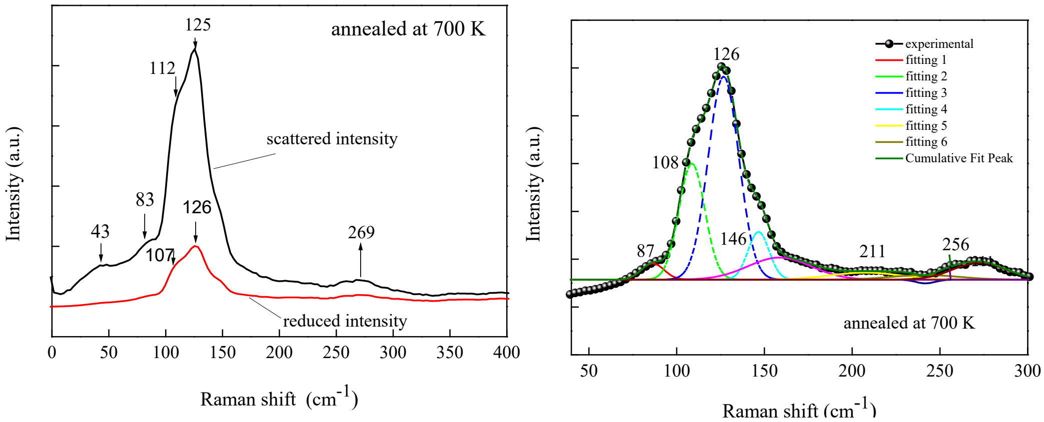

(a) *(b)*

Fig. 3. Raman spectra for $Ge_2Sb_2Te_5$ film annealed at 700 K (a) and Gaussian fitting (b).

The experimentally observed Raman shift at 300 K and the spectrum corresponding to the reduced intensity value (Fig. 1a), as well as the spectrum obtained in the Gaussian approximation (Fig. 1b) are shown in Fig. 1. The frequency of 45 cm^{-1} identified in reduced Raman intensity, also appears in the low-frequency regions of the corresponding spectrum for most amorphous materials and is considered a sign of the excitation of low-energy vibrational modes [1]. According to [22], the occurrence of low-frequency region (‘‘boson peak’’) in non-crystalline substances is comparable to the violation of selection rules for electronic transitions, caused by structural disorder. Gaussian fitting of the experimental data for the spectrum covering the region 75 ÷ 300 cm^{-1} related the vibrational modes presented in Table 1, where the integrated area of indicated peaks is given in brackets. According to the results from [1, 23], the peaks at 55 and 84 cm^{-1} obtained using the Gaussian fitting method correspond to the vibrational mode $G_3(E)$, which forms with the participation of three multiple coordinated Te atoms. The proposed interpretation of these vibrational modes is also supported by the findings in [24], where Gaussian approximations for $Ge_2Sb_2Te_5$ and GeTe layers in the low-frequency region of Raman shift show repeating patterns in peak distribution. Information about frequency of 91 cm^{-1} has also been mentioned in a number of works [1, 2, 23, 25], where this peak appears between 80 ÷ 90 cm^{-1} frequencies. The peak observed around 137 cm^{-1} also appears in works [1, 26]. The authors of [27] simulated the Raman scattering for amorphous $Ge_2Sb_2Te_5$ using empirical bond polarizability model and found that specified vibrational mode also exists in the spectrum of Sb_2Te_3. Thus, according to the findings of [27], it can be inferred that peak corresponds to vibrations of Sb-Te bonds in the defective octahedral arrangements of antimony atoms and pyramidal $SbTe_3$. In most published works there is not observed peak at 190 cm^{-1} (or 195 cm^{-1}) that we have noticed. Authors of [27] explain this fact by considering the unequal polarizability of the chemical bonds within the amorphous GST matrix. They argue that phonon density above 190 cm^{-1} is dominates due to vibrational modes that are forceful contained in tetrahedral of amorphous GST. However, they are not detected in Raman shift because polarizability of Ge-Te and Ge-Ge/Sb bonds in tetrahedral configurations is weaker than that of Sb-Te bonds in defective octahedral.

The weak Raman band observed in amorphous films around 220 cm^{-1} (in our experiments at 222 cm^{-1}) is assigned to F_2 mode in the tetrahedral $GeTe_4$ configuration [1]. The weak visibility of the vibrational modes of the $GeTe_4$ tetrahedron is related to its high symmetry compared to structural elements such as $GeTe_4$-nGe_n type (n = 1, 2) [1]. As previously mentioned, the structural arrangement of atoms in amorphous and crystalline GST ($Ge_2Sb_2Te_5$) films is distinctly different from that of most non-crystalline materials. Indeed, as shown in Figures 2-3, the Raman spectrum of amorphous GST undergoes a noticeable change as a result of heat treatment exceeding the crystallization temperature. These figures show the Raman spectra of GST films that subjected to thermal treatments at temperatures of 500 K (Fig. 2) and 700 K (Fig. 3). According to reference [15], under these thermal conditions, amorphous GST films progressively convert into closest packed cubic and hexagonal crystalline configuration.

The spectrum of reduced intensity spectral lines obtained after isothermal annealing at 500 K consists of four peaks at frequencies 53, 70, 115 and 153 cm^{-1} (Fig. 2a). The use of Gaussian approximation to experimentally observed spectral peaks allowed for the identification of 10 vibrational modes (Fig. 2b, Table 2), indicating the formation of new structural elements and chemical bonds as a result of crystallization induced by heat treatment. The existence of 48 and 65 cm^{-1} suggests a high degree of defectiveness in the cubic crystals (FCC) obtained by heat treatment at 500 K. According to [28-29] top at 65 cm^{-1} is coinciding with three-fold coordinated tellurium atom vibrations. The frequency of 108 cm^{-1} as reported by [14,24,30], appeared at 105 cm^{-1} after heat treatment at both 500 K and 700 K. The authors of the cited works attributed indicated peak to tetrahedral units of the type $GeTe_{4-n}Ge_n$ (n = 0, 1, 2). The 114 cm^{-1} frequency might right refer to A_1 symmetry of the indicated element with common angles, since its frequency is close to the peak at 120 cm^{-1}, which in several works [17, 24, 31, 32] has been associated with this structural element. The peaks observed at 152 and 167 cm^{-1} are assigned to the A_{1g}^2 mode in Sb_2Te_3 structural element [17]. The Raman spectrum of crystalline GST films after heat treatment at 700 K differs significantly from the spectrum recorded after heat treatment at 500 K (Fig. 3). In particular, peaks corresponding to the low-frequency vibrational modes are not observed in this spectrum. The noted features of the said spectrum obtained with such heat treatment of amorphous films indicate to establishment of an excellent crystal with a hexagonal configuration.

According to [25], during isothermal heat treatment at a temperatures above 500 K, the $GeTe_{4-n}Ge_n$ and Sb_mTe_3 (m = 1, 2) structural elements within $Ge_2Sb_2Te_5$ contribute only modestly to phase change under these parameters. Applying the Gaussian fitting method to the Raman spectra with reduced intensity spectral lines (Fig. 3), 6 peaks were identified (Table 1). The dominating 126 cm^{-1} frequency is close to the 120 cm^{-1} and as noted, indicates to A_1 mode of named tetrahedral units with common angles. The vibration at 146 cm^{-1} is linked to Sb-Te bond of pyramidal Sb_mTe_3 units type (m=1, 2) [24, 33-35]. In contrast to the mentioned study, in our case, the amplitude of 146 cm^{-1} was lower than that the magnitude at 126 cm^{-1}. The Raman resonance at 90 cm^{-1} (we have 87 cm^{-1}) is owing to E mode of $GeTe_4$ [17]. The 105 cm^{-1} frequency was also seen in Raman band of laser-crystallized $Ge_2Sb_2Te_5$ and, as mentioned earlier, was associated with tetrahedral units of the $GeTe_{4-n}Ge_n$ type. The maximums with 211 and 256 cm^{-1} affiliated with antisymmetric stretching modes of angle-sharing $GeTe_{4-n}Ge_n$tetrahedra [36].

Table 1. The bands of Raman frequencies observed in $Ge_2Sb_2Te_5$ films before and after annealing process.

Annealing temperature (K)	Wave number of vibrational modes (cм$^{-1}$) with integrated area value (J/g)									
300	50 (2713)	137 (11621)	195 (2493)	222 (438)	-	-	-	-	-	-
500	48 (2064)	65 (7200)	99 (7966)	108 (9548)	114 (9525)	152 (7617)	167 (6072)	190 (2908)	210 (1679)	214 (2252)
700	87 (4305)	108 21348	126 (34145)	146 (12272)	211 (3703)	256 (3607)	-	-	-	-

4. Processing of XRD spectrum data

The X-ray patterns of $Ge_2Sb_2Te_5$ (Fig. 4a) reveals that films prepared by thermal evaporation (before annealing) consist of broad bands, confirming their amorphous nature. The figure also indicates that heat treatment at a temperature of 400 K leads to partial crystallization of amorphous films. Heat treatment at 500 and 700 K results in polycrystalline films with cubic and hexagonal structures (Fig. 4b). The sizes of nanoparticles (crystallites) were calculated using Scherrer's equation based on the X-ray spectrum data, which relates size of crystallite with the width of diffraction maximum [18-20]:

$$D=\frac{K\lambda}{\beta cos\theta} . \qquad (2)$$

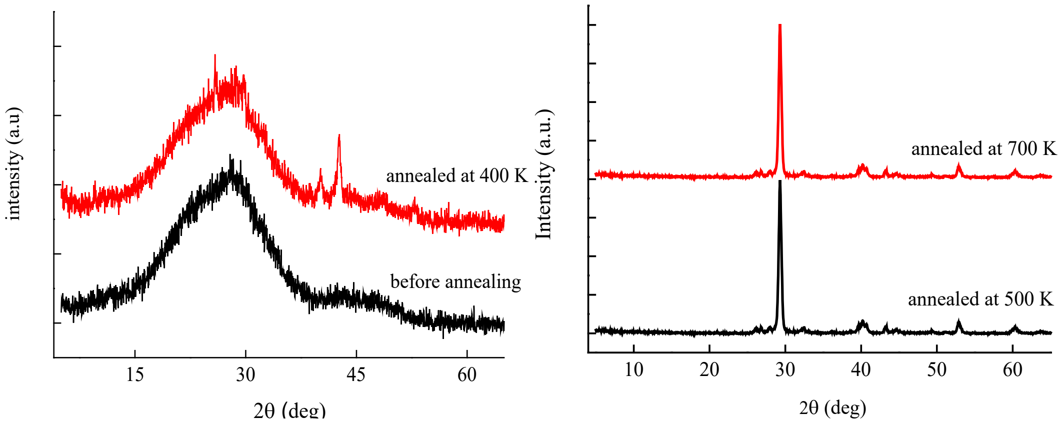

(a) *(b)*

Fig. 4. XRD patterns of $Ge_2Sb_2Te_5$ films before and after annealing process.

Table 2. Structure parameters of $Ge_2Sb_2Te_5$ from XRD annealed at 500 K determined by Scherrer's equation.

No	T (K)	2θ (degree)	FWHM (degree)	D_s (nm)	D_s (average, nm)	$d\times10^{-2}$ (Å)	$\delta_s\times10^{-2}$(nm^{-2})	$\varepsilon_s\times10^{-3}$	θ (°)
1	500	26,28627	11,89427	0,68415	10,9512	33,7895	213,649	222,2872	13,1431
2		28,38634	4,44136	1,84042		31,3346	29,5235	76,4697	14,1932
3		29,30669	0,4462	18,3571		30,3722	0,29675	7,445175	14,6534
4		32,4057	0,84888	9,72187		27,5343	1,05803	12,74485	16,2029
5		40,19715	1,1651	7,24389		22,3586	1,90570	13,88951	20,0986
6		43,26336	0,42033	20,2859		20,8431	0,24300	4,623947	21,6317
7		52,91892	0,53811	16,4586		17,2453	0,36915	4,716008	26,4595
8		60,30764	0,70453	13,0176		15,298	0,59011	5,28881	30,1539

Table 3. Structure parameters of $Ge_2Sb_2Te_5$ annealed at 700 K determined by Scherrer's equation.

No	T(K)	2θ (degree)	FWHM (degree)	D_s (nm)	D_s (average, nm)	$d\times10^{-2}$ (Å)	δ_s(nm^{-2})	$\varepsilon_s\times10^{-3}$	θ (°)
1	700	26,3741	1,20132	6,77492	11,6577	33,67873	2,178671	22,36976	13,18704
2		26,3741	11,9499	0,681079		33,67873	215,5783	222,5194	13,18704
3		29,0125	2,41682	3,386859		30,67214	8,717777	40,75385	14,50625
4		29,3071	0,43831	18,68772		30,36982	0,286344	7,313246	14,65353
5		32,3619	1,05092	7,851933		27,56979	1,621985	15,801	16,18091
6		40,1971	1,17416	7,18792		22,35929	1,935501	13,99828	20,09856
7		43,2627	0,42361	20,12885		20,84314	0,24681	4,659678	21,63133
8		44,5807	0,80702	10,61523		20,25719	0,887445	8,587407	22,29037
9		49,4113	0,36572	23,86204		18,38425	0,175624	3,467235	24,70565
10		52,9192	0,54329	16,30009		17,24539	0,376374	4,761024	26,4596
11		60,3077	0,7188	12,75815		15,298	0,614363	5,395841	30,15384

Using XRD data, the interplanar spacing (d -spacing) was determined, which is defined as the interatomic distance in angstroms. For this, we used the Bragg's equation $n\lambda = 2d sin\theta$, in which d is interplaner spacing or d-spacing (in Å) [19-20]. In this study, δ (nm^{-2}) - the dislocation density were calculated from XRD data by the formula $\delta = \frac{1}{D^2}$, and ε- the microstrain, coefficient characterizing the degree of structural distortion using the formula $\varepsilon = \frac{\beta}{4tan\theta}$ [20] end of which in Tables 2-3. The computed parameters from Tables 2-3 show that studied substance consists of nanosized crystallites (i.e. particles smaller than 100 nm), which indicate that reflection occurs not only at the Bragg angle. Therefore, broadening of the diffraction peaks is observed in the X-ray patterns, which will be more pronounced as the size of the crystallites decreases (Fig. 4).The diffraction peaks at the crystallite size (D) less than 5-10 nm in the X-ray patterns broaden so much that this substance becomes amorphous. Therefore, to assess the true structure and size of crystallites, the broadening of the diffraction reflections is analyzed. Based on the experimentally determined value of the true physical broadening of the line β (peak half-width or FWHM), the average size of crystallites D in the sample can be determined using Scherrer's equation. This analysis of the broadening and shape of the X-ray diffraction spectrum allows for a quantitative assessment of the polydispersity (distribution of crystallites by size) and defectiveness (structure of dislocation) in the analyzed substance.

As Tables 2 and 3 show, average size of crystallite (D) for $Ge_2Sb_2Te_5$ increases with rising annealing temperature. In the sample subjected heat treatment at 500 K, D = 10.9512 nm, while at 700 K, D = 11.6577 nm, indicating that partial phase transformation of structure occurs with temperature increasing. The Williamson-Hall method was also applied in the study to analyze the X-ray diffraction data (XRD). Using FWHM (β) data and peak position (θ, rad) from XRD, the Williamson-Hall plot (Fig. 5) was constructed and the size of crystallites ($D_{W\text{-}H}$) with the microstrain (ε) of the studied samples were determined [20-21].

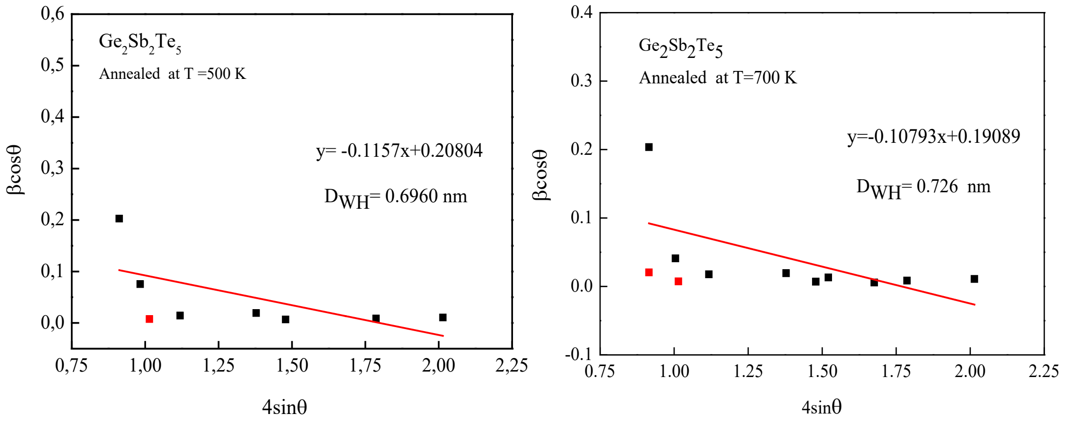

(a) *(b)*

Fig. 5. W-H plots of $Ge_2Sb_2Te_5$ annealed at temperatures of a) 500 K and b)700 K

In XRD, the peak broadening (β_T - total broadening) is caused both by the size of crystallites (β_D) and microstrain (β_ε) simultaneously ($\beta_T = \beta_D + \beta_\varepsilon$). The value of β_D or FWHM is determined from the Scherrer's equation [18-20], while β_ε is identical to $4\varepsilon\, tan\theta$. Thus, for the total broadening, we have:

$$\beta_T \times cos\theta = \varepsilon(4sin\theta) + \frac{K\lambda}{D}. \tag{3}$$

This is equivalent of the straightforward path, where ε is the line slope and $\frac{K\lambda}{D}$ instead of y-intercept.

Table 4. Parameters of $Ge_2Sb_2Te_5$ determined using Williamson-Hall method.

Annealing T (K)	Intercept $c = \frac{K\lambda}{D_{W-H}}$	$D_{W\text{-}H}$ (nm)	Slope m	Micro-strain $\varepsilon \times 10^{-2}$
500	0.20804	0.6960	-0.1157	-12
700	0.19089	0.726	-0.10793	-11

In figure 5, there is a plot with (4 sinθ) on x-axis, (β cosθ) on y –axis, and fitting gives a straight line. Numerical values for the size of crystallites and microstrain were found, with the results presented in table 4. The value of *m* in the table shows the difference in the line slope (gradient), thus identical to ε.

5. Conclusion

Amorphous $Ge_2Sb_2Te_5$ films with 0.3 ÷ 1 µm thickness have been obtained via thermal deposition of substance on glass surface with ~0.05 µm/min rate. The disordered nature in atoms arrangement of the films was verified via the striped distribution of intensity in the X-ray diffraction. Heat treatment at temperatures of 500 and 700 K leads to crystallization of films into successive cubic and hexagonal structures. It has been establised that as heat treatment temperature rises, the size of crystallites grows, while the dislocation densities and degree of structural distortion decrease; that is, the hexagonal structure obtained by heat treatment at 700 K is more perfect.

Using the Gaussian approximation to the Raman spectra with reduced intensity, the vibrational modes, chemical nature and main matrix elements of investigated $Ge_2Sb_2Te_5$ were determined. It was found that the dominant vibrational modes of the amorphous (at 300 K), as well as crystallized at temperatures of 500 and 700 K $Ge_2Sb_2Te_5$ material are 137, 109 and 126 cm^{-1}, respectively. The vibration around 137 cm^{-1} corresponds to Sb-Te bond in pyramidal $SbTe_3$ units. The extremes with 109 and 126 cm^{-1} frequency are attributed to softened A_1 mode of $GeTe_4$ and $GeTe_{4-n}Ge_n$ tetrahedral units with common bond angles.

Acknowledgements

The work was carried out at the Institute of Physics of Ministry of Science and Education, Republic of Azerbaijan.

References

[1] K.S. Andrikopoulos, S.N. Yannopoulos, G.A. Voyiatzis, A.V. Kolobov, M. Ribes, J. Tominaga, J. Phys.: Condens. Matter 18, 965 (2006); https://doi.org/10.1088/0953-8984/18/3/014
[2] K.S. Andrikopoulos, S.N. Yannopoulos, A.V. Kolobov, P. Fons, J. Tominaga, Journal of Physics and Chemistry of Solids, 68, 1074 (2007); https://doi.org/10.1016/j.jpcs.2007.02.027
[3] P. Jovari, I.Kaban, J. Steiner, B.Beuneu, A.Schöps, M.A. Webb, Phys. Rev. B**77**, 035202(1-6) (2008); https://doi.org/10.1103/PhysRevB.77.035202
[4] J. Hegedüs, S.R. Elliott, Nature Materials **7**, 399 (2008); https://doi.org/10.1038/nmat2157
[5] M. Naito, M. Ishimaru, Y. Hirotsu, R. Kojima, N. Yamada, Journal of Applied Physics 107**,** 103507 (2010); https://doi.org/10.1063/1.3373419
[6] P. Němec, V. Nazabal, A. Moreac, J. Gutwirth, L. Beneš, M. Frumar, Materials Chemistry and Physics 136, 935 (2012); https://doi.org/10.1016/j.matchemphys.2012.08.024
[7] K. Shportko,L. Revutska, O. Paiuk, J. Baran , A. Stronski, A. Gubanova, E. Venger,Optical Materials 73, 489 (2017); https://doi.org/10.1016/j.optmat.2017.08.042
[8] A. Piarristeguy, M. Micoulaut, R. Escalier, G. Silly, M.V. Coulet, A. Pradel, J. Non- Cryst. Solids 562, 120730 (2021); https://doi.org/10.1016/j.jnoncrysol.2021.120730
[9] Cinkaya Hatun, Ozturk Adil et all, Solid -State Electronics 185, 108101(2021); https://doi.org/10.1016/j.sse.2021.108101
[10]T.K. Nurubeyli, Inorganic Materials: Applied Research, 11, 552 (2020) https://doi.org/10.1134/S2075113320030351
[11] M. Wuttig, N. Yamada, Nature Materials 6, 824(2007); https://doi.org/10.1038/nmat2009
[12] W. Welnic, M. Wuttig, Materials Today 11 (6), 20(2008); https://doi.org/10.1016/S1369-7021(08)70118-4
[13] D. Lencer, M. Salinga, M. Wuttig, Adv. Mater. 23, 2030 (2011); https://doi.org/10.1002/adma.201004255
[14] P. Nemec, V. Nazabal, A. Moreac, J. Gutwirth, L. Benes, M. Frumar, Materials Chemistry and Physics 136, 935 (2012); http://dx.doi.org/10.1016/j.matchemphys.2012.08.024
[15] S.N. Garibova, A.I. Isaev, S.I. Mekhtieva, S. U. Ataeva, R.I. Alekberov. Semiconductor, 56, 175 (2022); https://doi.org/10.1134/S1063782622020063

[16]S. N. Garibova, A. I. Isayev, S. I. Mekhtiyeva, S. U. Atayeva, Semiconductor 53, 1507 (2019); https://doi.org/10.1134/S1063782619110071

[17] S. Kozyukhina, M. Veres, H. P. Nguyena A. Ingram, V. Kudoyarova,10th International Conference on Solid State Chemistry, Pardubice, Czech Republic., Physics Procedia 44, 82 (2013); https://doi.org/10.1016/j.phpro.2013.04.011

[18] F.T.L. Muniz, M. A. R. Miranda, C. Morilla dos Santos, J. M. Sasaki, Acta Cryst.A: Foundation and Advances 72, 385 (2016); https://doi.org/10.1107/S205327331600365X

[19] A.L. Patterson, Physical Review 56,978 (1939); https://doi.org/10.1103/PhysRev.56.978

[20] A. Monshi, M. R. Foroughi, M. R. Monshi, World Journal of NanoScience and Engineering 2, 3, 154 (2012); http://dx.doi.org/10.4236/wjnse.2012.23020

[21] K.K. Mustafa,A. J. Kareem, IOP Conference Series: Materials Science and Engineering 928, 072109, 1 (2020); http://dx.doi.org/10.1088/1757-899X/928/7/072109

[22] R. Shuker, R.W. Gammon, Phys. Rev. Lett., 25, 222 (1970); https://doi.org/10.1103/PhysRevLett.25.222

[23] R. Mazzarello, S. Caravati, S. Angioletti-Uberti, M. Bernasconi, M. Parrinello, Phys. Rev. Lett. 104, 85503 (2010); https://doi.org/10.1103/PhysRevLett.104.085503

[24] P. Nemec, A. Moreac, V. Nazabal, M. Pavlišta, J. Pikryl, M. Frumar, J.Appl. Phys. 106, 103509 (2009); https://doi.org/10.1063/1.3259435

[25] Jia Du, Zhangjian Mu, Lan Li, Junying Li,Optics & Laser Technology 144, 107393 (2021); https://doi.org/10.1016/j.optlastec.2021.107393

[26] G.C. Sosso, S. Caravati, R. Mazzarello, M. Bernasconi, Phys. Review B 83, 134201 (2011); https://doi.org/10.1103/PhysRevB.83.134201

[27] T. Wei, J. Wei, K. Zhang, H. Zhao, L. Zhang, Sci. Reports. 7 (1) (2017); https://doi.org/10.1038/srep42712

[28] H.R. Yoon, W. Jo, E. Cho, S. Yoon, M. Kim, J. Non-Crystal. Solids 352, 3757 (2006); https://doi.org/10.1016/j.jnoncrysol.2006.05.038

[29] M. Upadhyay, S. Murugavel, M. Anbarasu, T.R. Ravindran, J. Appl. Phys. 110, 083711 (2011); https://doi.org/10.1063/1.3653265

[30] G. Wang, Li. D. Shi, Y. Zhang, X. Shen, Spectrochimica Acta A: Mod. Biomol. Spectros.205, 551 (2018); https://doi.org/10.1016/j.saa.2018.07.077

[31] J. Fu, X. Shen, Y. Xu, G. Wang, Q. Nie, C. Lin, S. Dai, T. Xu, R. Wang, J. Mater. Lett. 88, 148 (2012); https://doi.org/10.1016/j.matlet.2012.08.051

[32] W. P. Zhou, F. R. Liu,, N. Bai, Y.H. Wan, X. Lin, J.M. Chen,Appl. Surf. Sci. 285, 97 (2013); https://doi.org/10.1016/j.apsusc.2013.07.082

[33] S. Kozyukhin, Y. Vorobyov, A. Sherchenkov, A. Babich, N. Vishnyakov, O. Boytsova, Physica St. Solidi (a) 213, 7, 1831 (2016); https://doi.org/10.1002/pssa.201532930

[34] Z. Xu, C. Chen, Z. Wang, K. Wu, H. Chong, H. Ye, RSC Adv. 8, 37, 21040 (2018); https://doi.org/10.1039/C8RA01382A

[35] S. Kozyukhin, P. Lazarenko, Y. Vorobyov, A. Baranchikov, V. Glukhenkaya, M. Smayev, A. Sherchenkov, Y. Sybina, A. Polohin, V. Sigaev, Opt. Laser Technol. 113,87 (2019); https://doi.org/10.1016/j.optlastec.2018.12.017

[36] S. Caravati, M. Bernasconi, T.D. Kühne, M. Krack, M. Parrinello, J. Phys. Condens. Matter 21, 255501 (2009); https://doi.org/10.1088/0953-8984/21/25/255501